 FDMP, vol.11, no.3, pp.279-300, 2015

Natural Convection in a Square Cavity Filled with Nanofluids

Abd el malik Bouchoucha[1,2], **Rachid Bessaïh**[1]

Abstract: The present paper deals with a numerical study of natural convection in a square cavity filled with a nanofluid. The left and right vertical walls of the cavity are maintained at a local temperature T_h (heat source) and a local cold temperature T_C, respectively. Horizontal walls are assumed to be adiabatic. The governing equations are discretized by using the finite volume method and solved by the SIMPLER algorithm. Our computer fortran code is validated through comparison with numerical results found in the literature. Results are presented in terms of streamlines, isotherms, local and average Nusselt numbers for the Rayleigh number ($10^3 \leq Ra \leq 10^6$), solid volume fraction of nanoparticles ($0 \leq \phi \leq 0.10$), type of nanofluids (Cu, Ag, Al_2O_3 and TiO_2), and dimensionless length of the heat source ($0.50 \leq B \leq 1$).

Keywords: Natural Convection, Nanofluid, Cavity.

Nomenclature

$A =$	surface, m^2
$B =$	dimensionless heat source length
$C_{P=}$	specific heat, J kg^{-1} K^{-1}
$g =$	gravitational acceleration, $m.s^{-2}$
$h =$	heat transfer coefficient, W m^{-2} K^{-1}
$k =$	thermal conductivity, Wm^{-1} K^{-1}
$L =$	cavity length, m
$Nu_s =$	local Nusselt number along the heat source
$Nu_m =$	average Nusselt number
$P =$	dimensionless pressure
$p =$	pressure, Pa
$Ra =$	Rayleigh number

[1] LEAP Laboratory, Department of Mechanical Engineering, Faculty of Sciences Technology, University Frères Mentouri-Constantine, Route de Ain El. Bey, Constantine 25000, Algeria.
[2] Email: bouchoucha.malik@gmail.com, Phone/Fax: +21331 811308

Pr = Prandtl number
T = Temperature, K
U, V = dimensionless velocity components
u, v = velocity components, m s^{-1}
X, Y = dimensionless Cartesian coordinates,m
x, y = Cartesian coordinates, m

Greek Symbols

α = thermal diffusivity, m^2 s^{-1}
β = thermal expansion coefficient, K^{-1}
ϕ = solid volume fraction
Θ = dimensionless temperature
μ = dynamics viscosity, kg $m^{-1}s^{-1}$
ν = kinematic viscosity, m^2s^{-1}
ρ = density, kg m^{-3}
ψ = dimensionless stream function

Subscripts

p = nanoparticle
nf = nanofluid
c = cold
h = hot

1 Introduction

Nano-scale particle added fluids are called as nanofluid, this technique was introduced by Choi (1995). Compared with the suspended particles of millimeters or higher, nanofluids have greater stability and rheological properties, higher thermal conductivity and negligible pressure drop. Nanofluids seem to constitute a very interesting alternative for electronic cooling applications, micro-electromechanical systems, process heating/cooling to energy conversion and supply and magnetic cooling, etc.

During the several past years, numerical studies of nanofluid free convection in a square cavity were well studied and discussed [Ho, Chen, and Li (2008); Mahmoudi and Sebdani (2012); Jmai, Ben-Beya, and Lili (2013); Tiwari and Das (2007); Ooi and Popov (2013)]. In particular, Aminossadati and Ghasemi (2009) have investigated free convection of nanofluid in a square cavity cooled from two vertical and horizontal walls and heated by a constant heat flux on its horizontal bottom wall. It was found that type of nanoparticles and the length and location of the heat source affected significantly the heat source maximum temperature. On another work, the authors studied natural convection in an isosceles triangular enclosure

with a heat source located at its bottom wall [Aminossadati and Ghasemi (2011)]. Khanafer, Vafai, and Lightstone (2003) investigated the heat transfer enhancement in a two-dimensional enclosure using nanofluids for various pertinent parameters. They tested different models for nanofluid density, viscosity, and thermal expansion coefficients. It was found that the suspended nanoparticles substantially increase the heat transfer rate at any given Grashof number. Cheng (2012a, 2012b, 2012c) studied a diversity of free convection such as non-Newtonian nanofluids about a vertical truncated cone in a porous medium. Cho, Chen, and Chen (2012) studied natural convection heat transfer performance in a complex-wavy-wall enclosed. The accomplished work confirms that the presented results of this study provide a useful insight into the natural convection heat transfer of nanofluids. Keblinski, Phillpot, Choi, and Eastman (2002) found that the thermal conductivity increase of nanofluids is due to the Brownian motion of particles, the molecular-level layering of the liquid at the liquid/particle interface, the nature of heat transport in the nanoparticles, and the effect of nanoparticle clustering. Saleh, Roslan, and Hashim (2002) numerically investigated heat transfer enhancement of nanofluid in a trapezoidal enclosure using water–Cu and water–Al_2O_3. Jou and Tzeng (2006) used nanofluids to enhance natural convection heat transfer in a two-dimensional rectangular enclosure for various pertinent parameters. They indicated that the solid volume fraction of nanofluids causes an increase in the heat transfer coefficient. Oztop, Abu-Nada, Varol, and Al-Salem (2011) numerically analyzed the problem of steady state natural convection in an enclosure filled with a nanofluid by using heating and cooling sinusoidal temperature profiles on one side. They found that the addition of nanoparticles into water affects the fluid flow and temperature distribution especially for higher Rayleigh numbers. Mahmoudi and Sebdani (2012) investigated the problem of free convection fluid flow and heat transfer of Cu–water nanofluid inside a square cavity having adiabatic square bodies at its center. The obtained results show that for all Rayleigh numbers with the exception of $Ra = 10^4$, the average Nusselt number increases with an increase in the volume fraction of the nanoparticles.

Natural convection heat transfer of water-based nanofluids in an inclined square enclosure has a very interesting case of study in the literature. The researchers investigated the effects of the inclination angle of the cavity, solid volume fractions, length of the constant heat flux heater [Ogut (2009); Abu-Nada and Oztop (2009)]. Mahmoodi and Hashemi (2012) studied natural convection of a nanofluid in C-shaped enclosures. Mahmoudi, Shahi, Shahedin, and Hemati (2011) treated natural convection cooling of two heat sources vertically attached to horizontal walls of an open cavity. It was observed that the flow field and temperature distributions inside the cavity are strongly dependent on the Rayleigh number and the position of the

heat sources.

The objective of this study is to investigate the steady laminar natural convection in a square cavity filled with nanofluids. The influence of relevant parameters such as the Rayleigh number, solid volume fraction, type of nanofluids, and heat source length on flow and thermal fields and on local and average Nusselt numbers are studied. This geometry has potential application in the cooling of electronic components.

This paper is organized as follows. Section 2 presents the geometry and mathematical model. Section 3 discusses the numerical method and code validation. Section 4 presents the results and discussion. Finally, a conclusion is given.

2 Mathematical formulation

2.1 Problem description

The three configurations considered in this study are shown in figures 1a-c. Each square cavity of dimension L is filled with pure water and a nanofluid. The left vertical wall is kept at a local hot temperature T_h, the right vertical wall is maintained at a local cold temperature T_C, and the remaining boundaries are adiabatic. The base fluid (water) used is incompressible, Newtonian fluid that satisfies the Boussinesq hypothesis, and the nanofluid is assumed to be incompressible and the flow is laminar. The thermo-physical properties of the nanofluid are constant, except for the variation of density, which is estimated by the Boussinesq hypothesis. The base fluid and spherical solid nanoparticles (Cu, Ag, Al_2O_3 and TiO_2) are in thermal balance. The thermo-physiques properties of the base fluid and nanoparticles are presented in Table 1.

Table 1: Thermo-physicl properties of water and nanoparticles.

	ρ ($kg{\cdot}m^{-3}$)	Cp ($J{\cdot}kg^{-1}{\cdot}k$)	k ($W{\cdot}m^{-1}{\cdot}k^{-1}$)	$\beta \times 10^{-5}$ (k^{-1})	$\alpha \times 10^{-6}$ (m^2/s)
Pure water	997.1	4179	0.613	21	0.147
Copper (Cu)	8933	385	401	1.67	116.31
Silver (Ag)	10500	235	429	1.89	171
Alumina (Al_2O_3)	3970	765	40	0.85	13.17
Titanium oxide (TiO_2)	4250	686.2	8.9538	0.9	3.07

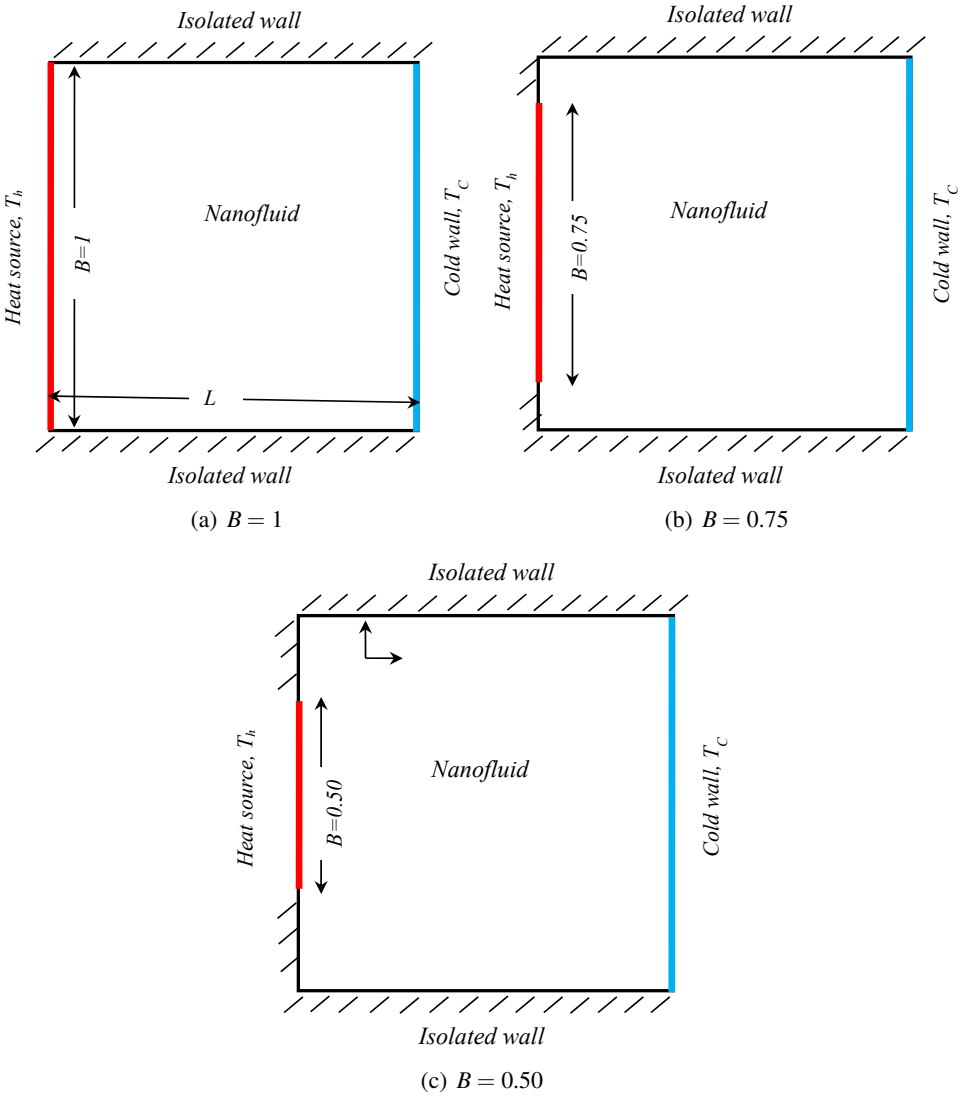

Figure 1: A schematic diagram of the physical model and boundary conditions. Here, L is the length of the cavity and B (normalized by L) the dimensionless length heat source: (a) $B = 1$, (b) $B = 0.75$, (c) $B = 0.50$.

2.2 Governing equations

The continuity, momentum and energy equations for the laminar and steady state natural convection in the two-dimensional cavity can be written in dimensional

form as follows:

$$\frac{\partial u}{\partial x}+\frac{\partial u}{\partial y}=0 \tag{1}$$

$$u\frac{\partial u}{\partial x}+v\frac{\partial u}{\partial y}=\frac{1}{\rho_{nf}}\left[-\frac{\partial p}{\partial x}+\mu_{nf}\left(\frac{\partial^2 u}{\partial x^2}+\frac{\partial^2 u}{\partial y^2}\right)\right] \tag{2}$$

$$u\frac{\partial v}{\partial x}+v\frac{\partial v}{\partial y}=\frac{1}{\rho_{nf}}\left[-\frac{\partial p}{\partial y}+\mu_{nf}\left(\frac{\partial^2 v}{\partial x^2}+\frac{\partial^2 v}{\partial y^2}\right)+(\rho\beta)_{nf}\,g\,(T-T_C)\right] \tag{3}$$

$$u\frac{\partial T}{\partial x}+v\frac{\partial T}{\partial y}=\alpha_{nf}\left(\frac{\partial^2 T}{\partial x^2}+\frac{\partial^2 T}{\partial y^2}\right) \tag{4}$$

The effective density of the nanofluid is given as:

$$\rho_{n_f}=(1-\phi)\,\rho_f+\phi\rho_p \tag{5}$$

where ϕ is the solid volume fraction of nanoparticles.
The thermal diffusivity of the nanofluid is

$$\alpha_{n_f}=k_{nf}/\,(\rho Cp)_{nf} \tag{6}$$

where, the heat capacitance of the nanofluid is given by:

$$(\rho Cp)_{n_f}=(1-\phi)\,(\rho Cp)_f+\phi\,(\rho Cp)_p \tag{7}$$

The thermal expansion coefficient of the nanofluid can be determined by

$$(\rho\beta)_{n_f}=(1-\phi)\,(\rho\beta)_f+\phi\,(\rho\beta)_p \tag{8}$$

The effective dynamic viscosity of the nanofluid given by Brinkman (1952) is:

$$\mu_{nf}=\frac{\mu_f}{(1-\phi)^{2.5}} \tag{9}$$

In Equation (2), k_{nf} is the thermal conductivity of the nanofluid, which for spherical nanoparticles, according to Maxwell (1881) is:

$$k_{\mathrm{nf}}=\left[\frac{(k_p+2k_f)-2\phi\,(k_f-k_p)}{(k_p+2k_f)+\phi\,(k_f-k_p)}\right] \tag{10}$$

In order to cast the governing equations into a dimensionless form, the following dimensionless parameters are introduced:

$$X=\frac{x}{L},\;\; Y=\frac{y}{L},\;\; U=\frac{uL}{\alpha_f},\;\; V=\frac{vL}{\alpha_f},\;\; P=\frac{pL^2}{\rho_{nf}\alpha_2^f},\;\; \theta=\frac{T-T_C}{T_h-T_C}$$

The non-dimensional continuity, momentum and energy equations are written as follows:

$$\frac{\partial U}{\partial X}+\frac{\partial V}{\partial Y}=0 \tag{11}$$

$$U\frac{\partial U}{\partial X}+V\frac{\partial U}{\partial Y}=-\frac{\partial P}{\partial X}+\frac{\mu_{nf}}{\rho_{nf}\alpha_f}\left(\frac{\partial^2 U}{\partial X^2}+\frac{\partial^2 U}{\partial Y^2}\right) \tag{12}$$

$$U\frac{\partial V}{\partial X}+V\frac{\partial V}{\partial Y}=-\frac{\partial P}{\partial Y}+\frac{\mu_{nf}}{\rho_{nf}\alpha_f}\left(\frac{\partial^2 V}{\partial X^2}+\frac{\partial^2 V}{\partial Y^2}\right)+\frac{(\rho\beta)_{n_f}}{\rho_{nf}\beta_{nf}}Ra\,\mathrm{Pr}\,\theta \tag{13}$$

$$U\frac{\partial \theta}{\partial X}+V\frac{\partial \theta}{\partial Y}=\frac{\alpha_{nf}}{\alpha_f}\left(\frac{\partial^2 \theta}{\partial X^2}+\frac{\partial^2 \theta}{\partial Y^2}\right) \tag{14}$$

$Ra=\frac{g\beta_f L^3(T_h-T_C)}{\nu_f\alpha_f}$ and $\mathrm{Pr}=\frac{\nu_f}{\alpha_f}$ are the Rayleigh and Prandtl numbers, respectively.

2.3 Boundary conditions

The dimensionless boundary conditions are:

At $X=0$: $U=V=0$, $\theta=1$ (heat source)

At $X=1$: $U=V=0$, $\theta=0$ (cold wall)

At $Y=0$: $U=V=0$, $\dfrac{\partial\theta}{\partial Y}=0$ (adiabatic wall)

At $Y=1$: $U=V=0$, $\dfrac{\partial\theta}{\partial Y}=0$ (adiabatic wall)

2.4 Local and average Nusselt numbers

The local Nusselt number on the heat source surface is defined as:

$$\mathrm{Nu}=\frac{hL}{k_f} \tag{15}$$

where h is he heat transfer coefficient.

By using the dimensionless variables mentioned above, the local Nusselt number becomes:

$$\mathrm{Nu}=-\frac{k_{nf}}{k_f}\left(\frac{\partial\theta}{\partial X}\right)_{wall} \tag{16}$$

where θ and X are the dimensionless temperature and coordinate, respectively. Finally, the average Nusselt number Nu_m along the heat source surface A can be obtained as:

$$\mathrm{Nu_m}=\frac{1}{A}\int NudA \tag{17}$$

3 Numerical method and code validation

The governing equations presented in Eqs. (11)–(14) along with the boundary conditions are solved by using FORTRAN code, which using a control volume formulation [Patankar (1980)]. The numerical procedure called SIMPLER [Patankar (1980)] is used to handle the pressure-velocity coupling. For treatment of the convection and diffusion terms in equations (12)–(14), the power-law and central difference schemes are adopted. The convergence was obtained when the energy balance between the heat source and the cold wall is less than a prescribed accuracy value, i.e., 0.1%.

3.1 Grid independence study

The study was undertaken to six grids: 122×122, 132×132, 142×142, 152×152 and 162×162, 172×172 nodes. Table 2 shows the variation of the maximum values Nu_m with grid size for Cu-water nanofluid, $B = 1$, $\phi = 0.1$, and $Ra = 10^5$. The changes in the calculated values are very small for three 152×152, 162×162, 172×172 grids and we noticed that the variation of Nu_m between 152×152 and 162×162 nodes is less than 0.001248 (see Table 2). However, and after running tests of independence between the numerical solution and the mesh, the fourth grid 152×152 nodes was chosen to complete the calculations. This grid also gives the best compromise between cost and accuracy of calculations.

Table 2: Grid independency results (Cu-water nanofluid, $B = 1$, $\phi = 0.1$, and $Ra = 10^5$).

Grid	122×122	132×132	142×142	152×152	162×162	172×172
Nu_m	5.251923	5.250128	5.248814	5.247566	5.246435	5.248814

3.2 Code validation

To verify the accuracy of the present numerical study, the numerical code was validated in two steps:

(1) With the numerical results of Aminossadati and Ghasemi (2009) at $Ra = 10^5$, $\phi = 0$ and 0.10 for the local Nusselt number Nu (Fig.2a) and the dimensionless temperature θ_S along the heat source (Fig.2b);

(2) With the work of Oztop and Abu-nada (2009) at $Ra = 10^5$ and $\phi = 0.10$ (Cu–water nanofluid) for the vertical velocity profile along the midsection of the enclosure (Fig.3a) and the average Nusselt number Nu_m with ϕ (Fig.3b). As shown in Figures 2a-b and 3a-b, it is clear that our results are in good agreement with the

numerical results of references Aminossadati and Ghasemi (2009) and Oztop and Abu-nada (2009).

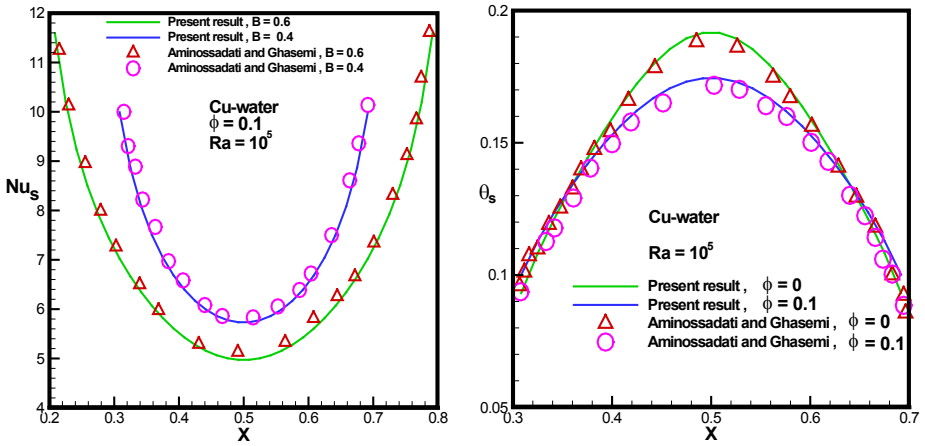

(a) (b)

Figure 2: Comparison between our results and those of Aminossadati and Ghasemi (2009) at $Ra = 10^5$, $\phi = 0$ and 0.10: (a) Local Nusselt number Nu_S along the heat source and (b) dimensionless temperature θ_S along the heat source.

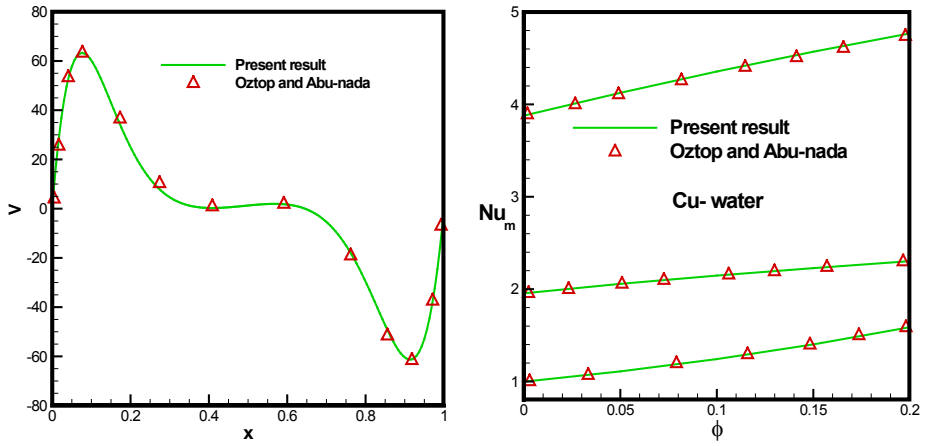

(a) (b)

Figure 3: Comparison between our results and those of Oztop and Abu-nada (2009) at $Ra = 10^5$ and $\phi = 0.10$ (Cu–water nanofluid): (a) Vertical velocity profile along the mid-section of the enclosure and (b) Average Nusselt number Nu_m with ϕ.

4 Results and discussion

The steady state results presented in this paper are generated for different parameters: ($10^3 \leq Ra \leq 10^6$), solid volume fraction of nanoparticles ($0 \leq \phi \leq 0.10$), type of nanofluids (Cu, Ag, Al_2O_3 and TiO_2), and dimensionless length of the heat source ($0.50 \leq B \leq 1$), and. The study deals with the effects of the Rayleigh number, solid volume fraction, type of nanofluids, and the heat source length on the flow structure, the components of the velocity, the temperature field, and the local and average Nusselt numbers along the heat source. The numerical results are presented in terms of streamlines, isotherms, profiles of horizontal and vertical velocity, and local and average Nusselt numbers.

4.1 Effects of Rayleigh number and solid volume fraction

Figure 4 shows streamlines (left) and isotherm (right) for a square cavity filled with Cu–water nanofluid (at $\phi = 0.1$) for different heat source lengths. For $Ra = 10^3$, we observe that the flow is symmetric and for $Ra = 10^4$ (figure 5) the flow is asymmetric in all cases. For the iso-contours of streamlines, we observed two circulating cell counter rotation for all cases and this is justified by the buoyancy force effect. Also, for $Ra = 10^4$ (figure 5) we can observe that the cell shape does not change and the solid volume fraction effect shows that the intensity of the iso-contours of streamlines augment with increasing of the volume fraction, as a result of high energy transport flows through the ultrafine particles. For $Ra = 10^4$, 10^5 and 10^6 (Figures 5–7), we notice that the fluid flow is asymmetry. In addition, this asymmetry is accompanied by an increase in the flow intensity and a reduction in the size of two vortexes, which move to the cavity side with, streamlines perturbation.

Figure 4 shows also the impact of the nanoparticle and the heat source length on the isotherm contours for Cu-water nanofluid. We note that the isotherms in the cavity center are horizontal (stratification in the vertical direction), with the formation of the thermal boundary layer along the vertical walls, which is due to the presence of nanoparticles and their solid volume fraction. This is justified by the thermal conductivity effect of nanoparticles, and we note that the best distribution obtained when the heat source length is equal to 1 ($B = 1$).

Figures 5–7 display a significant effect of Rayleigh number on the flow structure and temperature field in the square cavity. We show that, with the increase of Rayleigh number the effect of free convection increases with the increase of the thermal boundary layer just beside vertical walls. Furthermore, we observe that the increase in the solid volume fraction of the nanoparticle and thermal conductivity of nanofluid causes an increase of the thermal boundary layer.

Figure 8 illustrates the variation of the average Nusselt number ratio Nu_m^* (defined

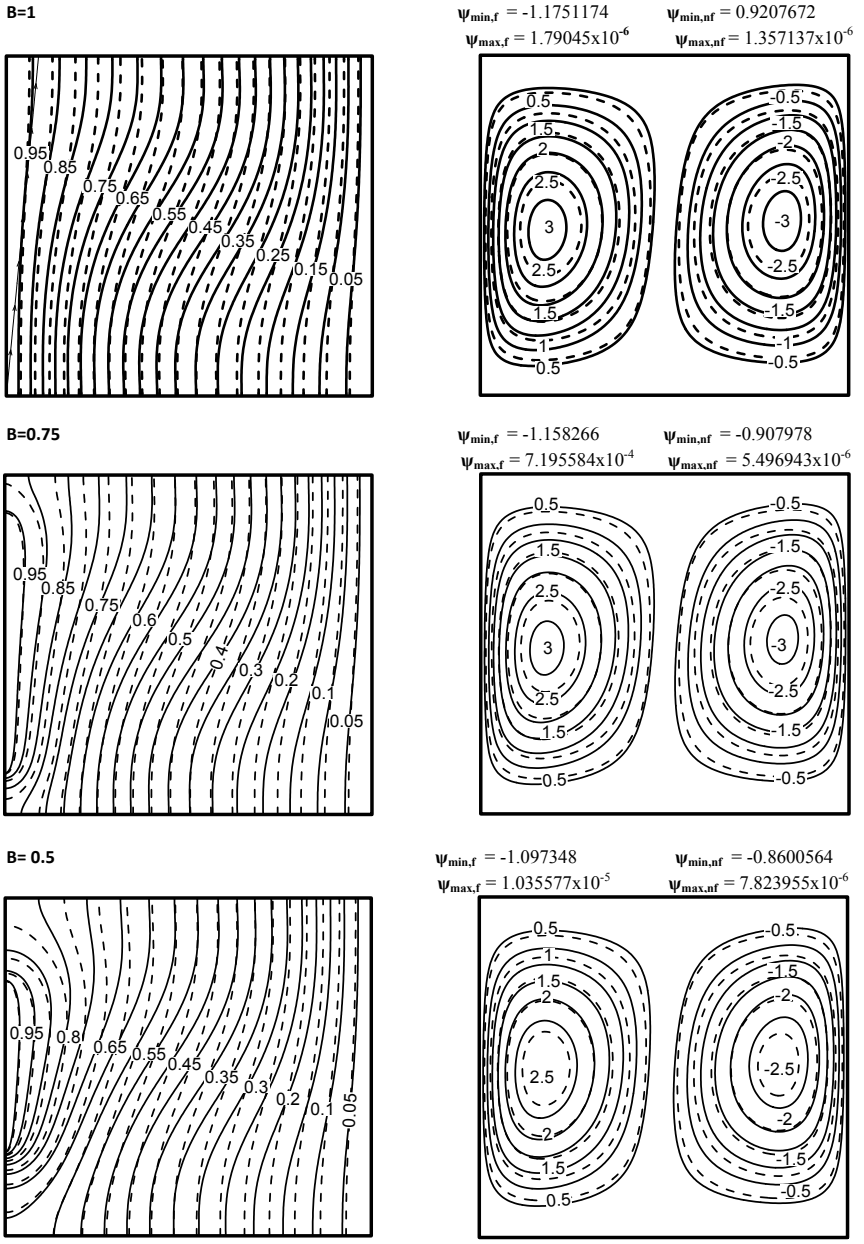

Figure 4: Isotherms (left) and streamlines (right) for the enclosures filled with Cu–water nanofluid $\phi = 0.1$ (—) and pure water $\phi = 0$ (- - - -) at $Ra = 10^3$ and different dimensionless heat source lengths B.

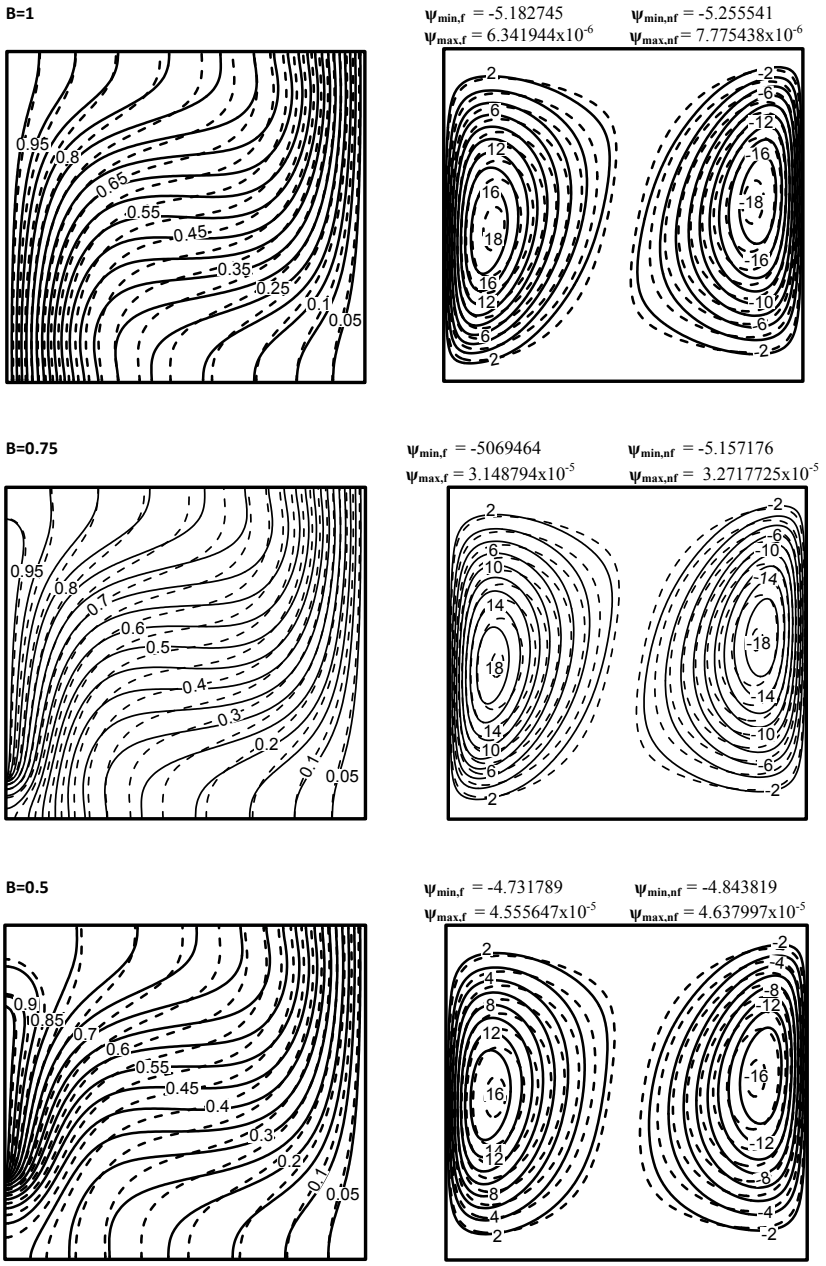

Figure 5: Isotherms (left) and streamlines (right) for the enclosures filled with Cu–water nanofluid $\phi = 0.1$ (—) and pure water $\phi = 0$ (- - - -) at $Ra = 10^4$ and different dimensionless heat source lengths B.

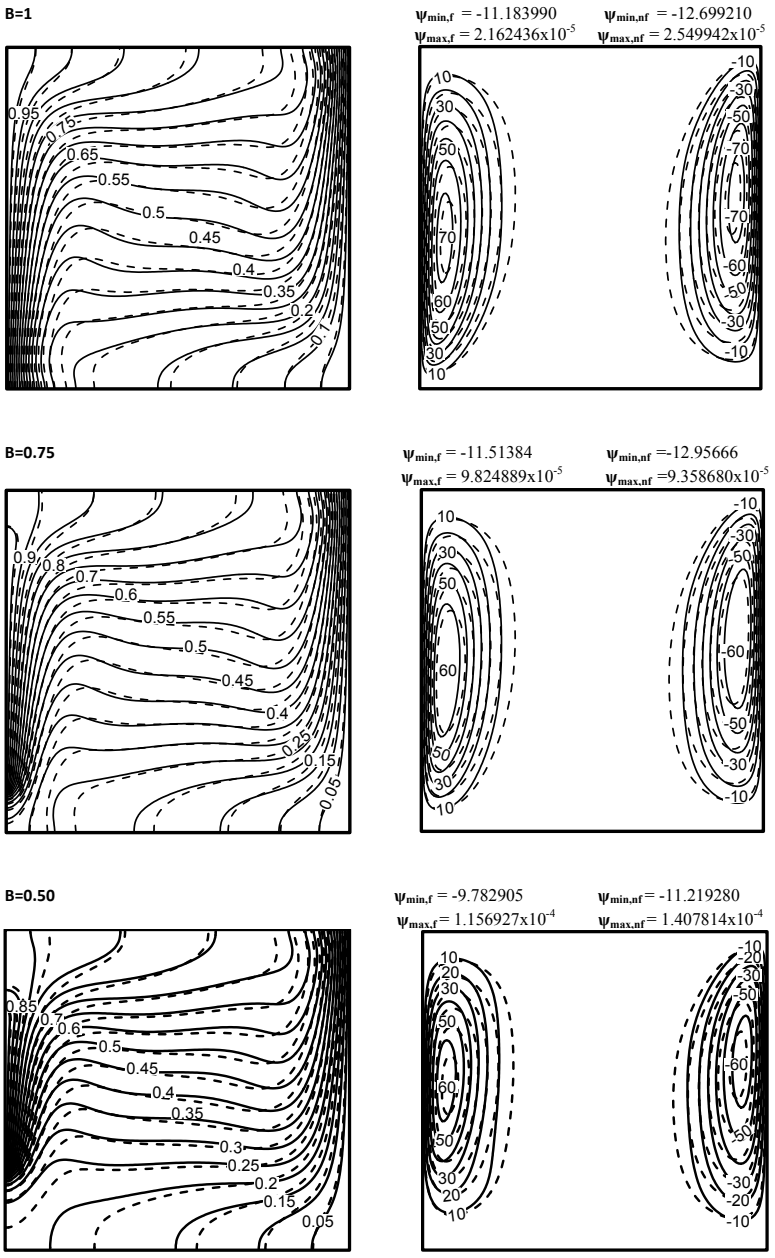

Figure 6: Isotherms (left) and streamlines (right) for the enclosures filled with Cu–water nanofluid $\phi = 0.1$ (—) and pure water $\phi = 0$ (- - - -) at $Ra = 10^5$ and different dimensionless heat source lengths B.

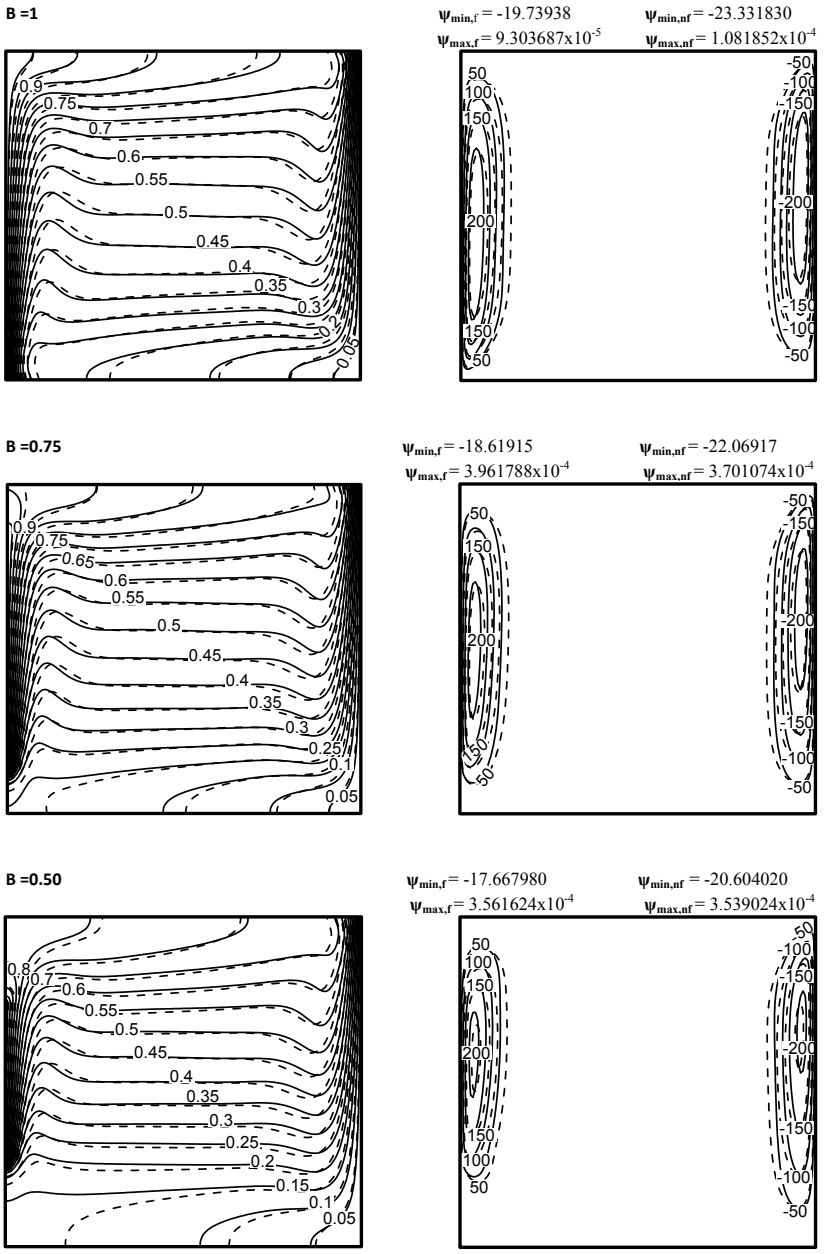

Figure 7: Isotherms (left) and streamlines (right) for the enclosures filled with Cu–water nanofluid $\phi = 0.1$ (—) and pure water $\phi = 0$ (- - - -) at $Ra = 10^6$ and different dimensionless heat source lengths B.

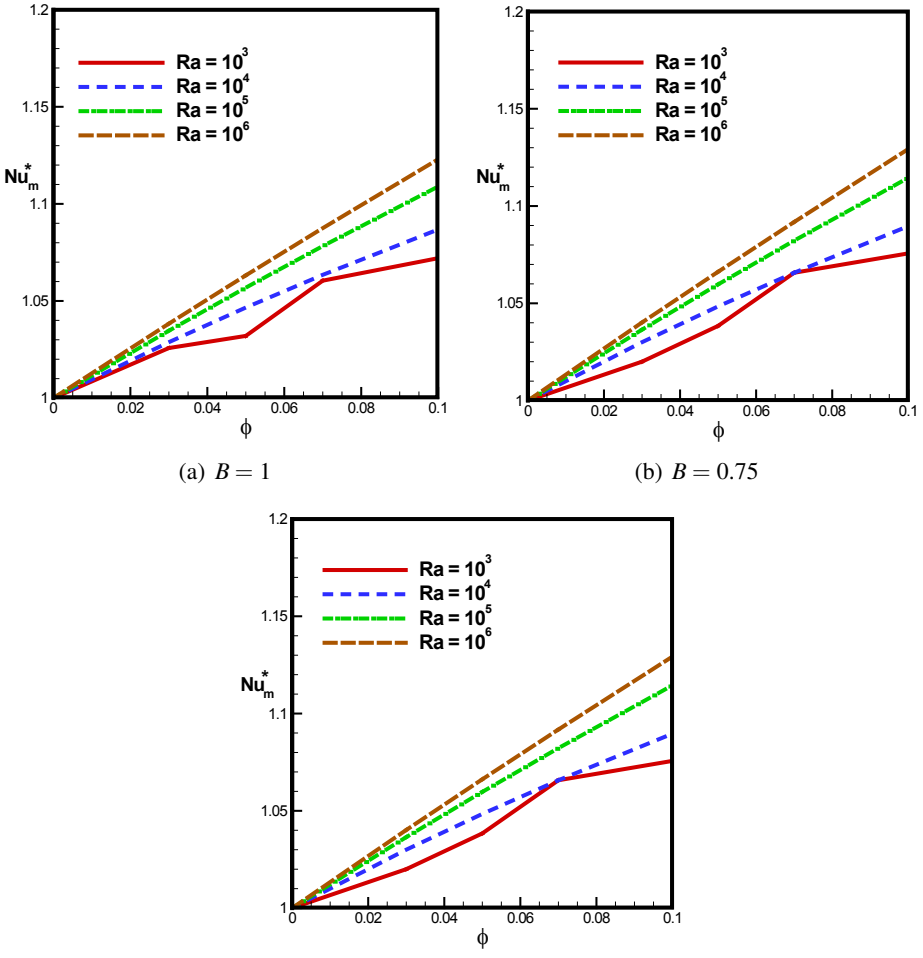

(a) $B = 1$

(b) $B = 0.75$

(c) $B = 0.5$

Figure 8: Variation of average Nusselt number ratio Nu_m^* ($= \mathrm{Nu}_{m\,(\phi\neq 0)}/\mathrm{Nu}_{m\,(\phi=0)}$) with solid volume fraction ϕ at various Rayleigh numbers and different dimensionless heat source lengths B. Here, $\mathrm{Nu}_{m\,(\phi\neq 0)}$ and $\mathrm{Nu}_{m\,(\phi=0)}$ are calcultated with a nanofluid and with pure water, respectively.

as: $\mathrm{Nu}_{m\,(\phi\neq 0)}/\mathrm{Nu}_{m\,(\phi=0)}$) with solid volume fraction ϕ at various Rayleigh numbers and different dimensionless heat source lengths B. We show that the average Nusselt number is independent at $Ra < 10^3$. In this case, we note the improved average Nusselt number with the increasing the volume fraction of nanoparticles. This is due to the enhancement of the effective thermal conductivity of the nanofluid with the increasing of the volume of nanoparticles. It is found that the addition

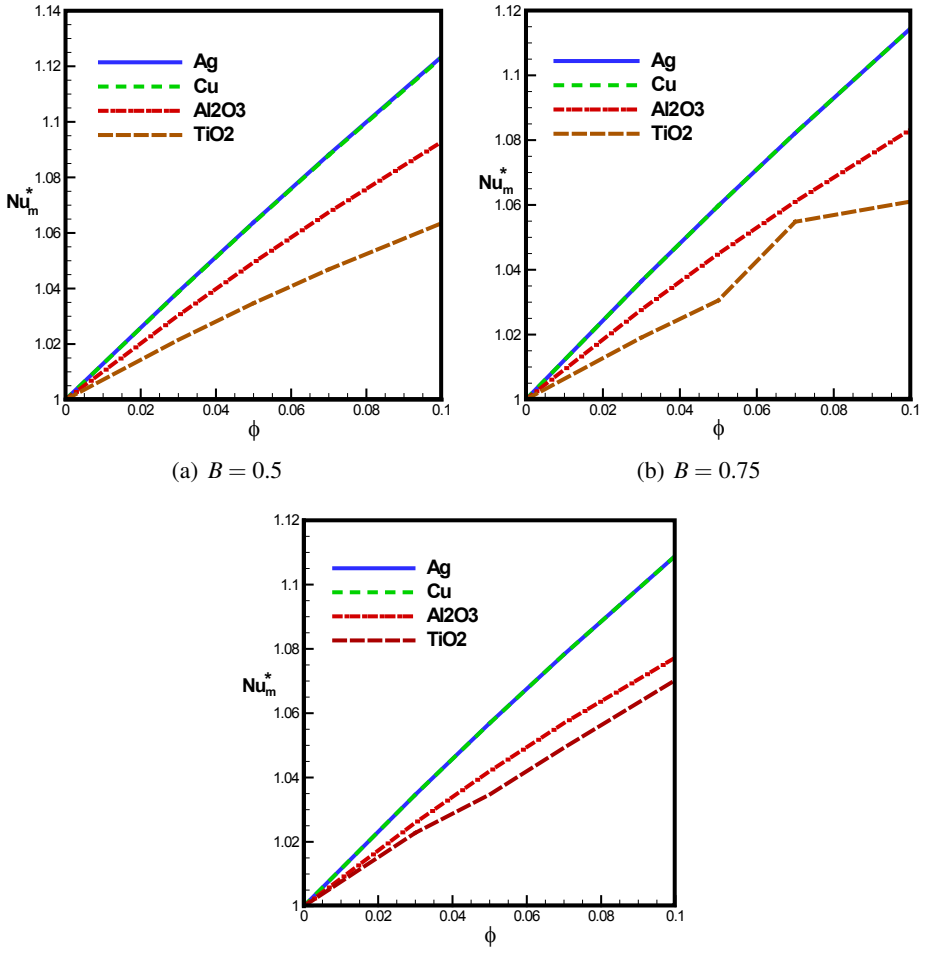

(a) $B = 0.5$ (b) $B = 0.75$

(c) $B = 1$

Figure 9: Variation of average Nusselt number ratio Nu_m^* with solid volume fraction ϕ for different dimensionless heat source lengths B at $Ra = 10^5$ and various nanofluids.

of nanoparticles improves the average Nusselt number, and the heat transfer inside the cavity is dominated by the conduction regime effect. For ($10^3 < Ra < 10^4$), the average Nusselt number increases in a non-linear way with the increasing of Rayleigh number, because the heat transfer is associated with conduction and convection regime effect. For $Ra > 10^4$, the average Nusselt number increases linearly with the increase of Rayleigh number. This is justified by the high buoyancy forces effects, and the heat transfer inside the cavity is dominated by convection. In addi-

tion, the highest values for Nusselt number are found at $Ra = 10^6$, where a stronger buoyant flow field appears in the enclosure. In addition, we can observe that the highest and lowest values of the average Nusselt number are obtained for $B = 0.5$ and 1, respectively. All figures show that the Nusselt numbers are starting from the same value. It is worth remarking that, the Rayleigh number values move away according to the solid volume increasing.

4.2 Effect of type of nanofluids

Figures 9a-c show the variation of the average Nusselt number ratio with solid volume fraction ϕ for different dimensionless heat source lengths B at $Ra = 10^5$ and various nanofluids. We show that the average Nusselt number ratio increases almost monotonically with increasing concentration for all nanofluids. At $Ra = 10^5$, we find the increase in the average Nusselt number ratio with the augmentation of the nanoparticles volume fraction, and this is justified by the increased of heat transfer mode by convection. In addition, we see that the average Nusselt ratio decreases as a function of the nanoparticle type (Ag, Cu, Al_2O_3, TiO_2), and the lowest value of the average Nusselt ratio is obtained for TiO_2 nanoparticles. This can be justified by the effect of the heat transfer mode by conduction and their low thermal conductivity compared to the other type of nanoparticle. However, the difference between the values of the average Nusselt ratio of Ag and Cu is negligible. This is due to the thermal conductivity effect of the nanoparticle type as it has shown in Table 1. In addition, we show that the average Nusselt number of the Ag and Cu nanoparticle are similarly for the heat source length $B = 1$ and 0.75. We conclude that the highest value of the average Nusselt ratio is obtained for the type Ag nanoparticle and a length of heat source $B = 0.5$.

Figure 10 shows the profile of local Nusselt number Nu_S along the heat source for various solid volume fractions ϕ at $Ra = 10^5$ and Cu–water nanofluid. We notice that the local Nusselt number takes highest solid volume fraction values, which fact leads to its increasing. Therefore, the local Nusselt number increasing is depending to the solid volume fraction increasing.

4.3 Effect of solid volume fraction

Figure 11 shows the vertical velocity profiles V at $Y = 0.50$ for various solid volume fractions ϕ at $Ra = 10^5$ and Cu–water nanofluid. We can notice that, the velocity profiles are inversed, which indicate the flow rotation direction. It is worth remarking that, the flow rises on the left side and descends near the vertical wall. It is also obviously clear that the absolute vertical velocity magnitude increases with the maximum temperature. In addition, the velocity increases according to the solid volume fraction increasing.

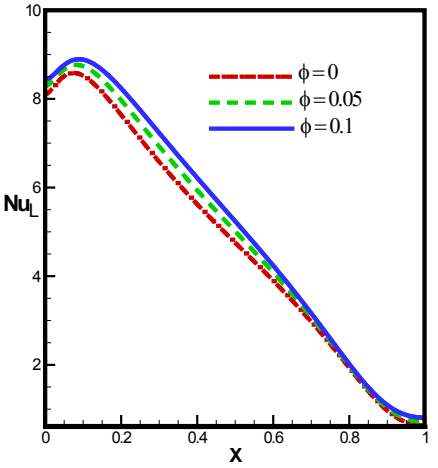

Figure 10: Profile of local Nusselt number Nu_S along the heat source for various solid volume fractions ϕ at $Ra = 10^5$ and Cu–water nanofluid.

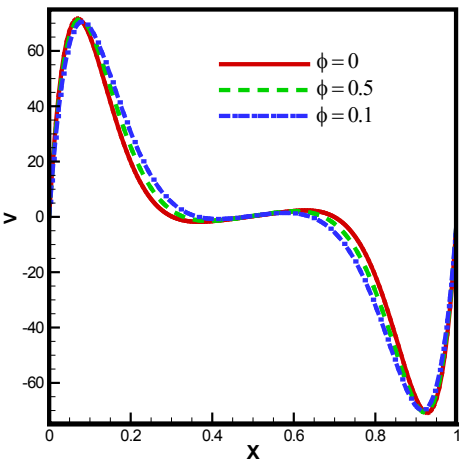

Figure 11: Vertical velocity profiles V at $Y = 0.50$ for various solid volume fractions ϕ at $Ra = 10^5$ and Cu–water nanofluid.

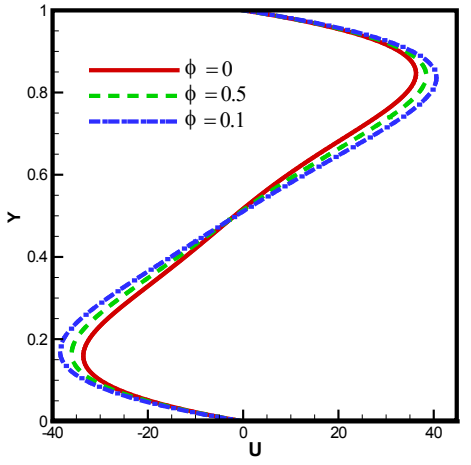

Figure 12: Horizontal velocity profiles U at $X = 0.50$ for various solid volume fractions ϕ at $Ra = 10^5$ and Cu–water nanofluid.

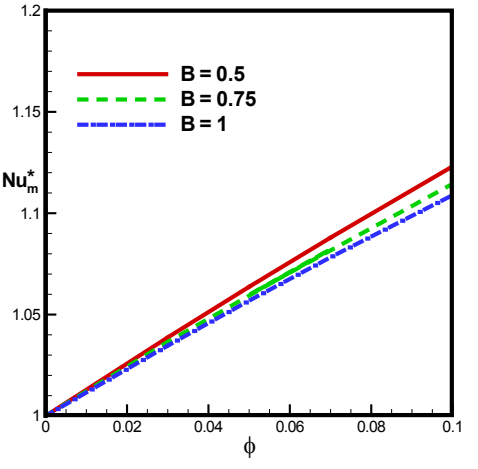

Figure 13: Variation of average Nusselt number ratio Nu_m^* with solid volume fraction ϕ for different dimensionless heat source lengths B at $Ra = 10^5$.

Figure 12 presents the horizontal velocity profiles U at $X = 0.50$ for various solid volume fractions ϕ at $Ra = 10^5$ and Cu–water nanofluid. It can be seen asymmetric

flow for a median plane of the cavity. The flow velocity along the middle of the cavity is equal to zero when the heat source is located to the left wall. The circulating cell on the left side of the cavity becomes limited as the heat source moves towards the left side of the bottom wall. Consequently, the right circulating cell grows and moves towards the center of the cavity. The velocity in the enclosure axis for the highest value of the Rayleigh number is very small compared to the limits levels ones where the fluid is moving with high velocities. This behavior presents a single-phase flow. As the solid volume fraction increases, the velocity components of nanofluid increase because of an increase in the energy transport during the fluid. High velocity peaks of the vertical velocity are illustrated in this figure at high volume fractions, when the heat source moves towards the middle, the maximum velocity increases significantly.

4.4 Effect of different heat source lengths

Figure 13 displays the variation of the average Nusselt number ratio with solid volume fraction ϕ for different dimensionless heat source lengths B at $Ra = 10^5$. We observe that in all cases ($B = 0.5$, 0.75, and 1), the average Nusselt number rate increases linearly with the increase of volume concentration. It concluded that a high Rayleigh number is introduced by a strong buoyancy effect, and therefore, the transfer of heat inside the enclosure is dominated by convection. Note that average Nusselt rate increases with the decrease in length of the heat source.

5 Conclusions

A numerical simulation of two-dimensional laminar natural convection in a square cavity filled with nanofluids has been carried out. A comparison with previously published work was performed and the results were to be in good agreement. The important concluding remarks are presented below:

- The effect of previous parameters has considerable effects on the flow and heat transfer inside the cavity.
- The average Nusselt number increases with an increasing volume fraction of nanoparticles. The results also show that, the Cu-water nanofluid gives good performance of heat transfer.
- The average Nusselt rate increases with the decrease in length of the heat source.

Acknowledgement: Mr. A. Bouchoucha (Doctorate student) gratefully acknowledges the financial support provided by the Algerian Ministry of Higher Education

and Scientific Research.

References

Abu-Nada, E.; Oztop, F. (2009): Effects of inclination angle on natural convection in enclosures filled with Cu–water nanofluid. *International Journal of Heat and Fluid Flow*, vol. 30, pp. 669–678.

Aminossadati, S. M.; Ghasemi, B. (2009): Natural convection cooling of a localised heat source at the bottom of a nanofluid-filled enclosure. *European Journal of Mechanics B/Fluids*, vol. 28, pp. 630–640.

Aminossadati, S. M.; Ghasemi, B. (2011): Enhanced natural convection in an isosceles triangular enclosure filled with a nanofluid. *Computers and Mathematics with Applications*, vol. 61, pp. 1739–1753.

Brinkman, H. C. (1952): The viscosity of concentrated suspensions and solutions. *J. Chemical Physics*, vol. 20, pp. 571.

Choi, S. U. S. (1995): Enhancing thermal conductivity of fluids with nanoparticles. *ASME Fluids Eng. Division*, vol. 231, pp. 99–105.

Cheng, C. Y. (2012a): Free convection of non-newtonian nanofluids about a vertical truncated cone in a porous medium. *International Communications in Heat and Mass Transfer*, vol. 39, pp. 1348–1353.

Cheng, C. Y. (2012b): Free convection boundary layer flow over a horizontal cylinder of elliptic cross section in porous media saturated by a nanofluid. *International Communications in Heat and Mass Transfer*, vol. 39, pp. 931–936.

Cheng, C. Y. (2012c): Natural convection boundary layer flow over a truncated cone in a porous medium saturated by a nanofluid. *International Communications in Heat and Mass Transfer*, vol. 39, pp. 231–235.

Cho, C. C.; Chen, C.-L.; Chen, C. (2012): Natural convection heat transfer performance in complex-wavy-wall enclosed cavity filled with nanofluid. *International Journal of Thermal Sciences*, vol. 60, pp. 255–263.

Ho, C. J.; Chen, M. W.; Li, Z. W. (2008): Numerical simulation of natural convection of nanofluid in a square enclosure: effects due to uncertainties of viscosity and thermal conductivity. *International Journal of Heat and Mass Transfer*, vol. 51, pp. 4506–4516.

Jmai, R.; Ben-Beya, B.; Lili, T. (2013): Heat transfer and fluid flow of nanofluid-filled enclosure with two partially heated side walls and different nanoparticles. *Superlattices and Microstructures*, vol. 53, pp. 130–154.

Jou, R. Y.; Tzeng, S. C. (2006): Numerical research of natural convective heat transfer enhancement filled with nanofluids in rectangular enclosures. *International Communications in Heat and Mass Transfer*, vol. 33, pp. 727–736.

Khanafer, K.; Vafai, K.; Lightstone, M. (2003): Buoyancy-driven heat transfer enhancement in a two-dimensional enclosure utilizing nanofluids. *International Journal of Heat and Mass Transfer*, vol. 46, pp. 3639–3653.

Keblinski, P.; Phillpot, S. R.; Choi, S. U. S; Eastman, J. A. (y2002): Mechanism of heat flow in suspensions of nano-sized particles (nanofluids). *International Journal of Heat and Mass Transfer*, vol. 45, pp. 855–863.

Mahmoudi, M.; Sebdani, S. M. (2012): Natural convection in a square cavity containing a nanofluid and an adiabatic square block at the center. *Superlattices and Microstructures*, vol. 52, pp. 261–275.

Mahmoudi, A.; Sebdani, A. (2012): Natural convection in a square cavity containing a nanofluid and an adiabatic square block at the center. *Superlattices and Microstructures*, vol. 52, pp. 261–275.

Mahmoodi, M.; Hashemi, S. M. (2012): Numerical study of natural convection of a nanofluid in c-shaped enclosures. *International Journal of Thermal Sciences*, vol. 55, pp. 76–89.

Mahmoudi, A.; Shahi, M.; Shahedin, A.; Hemati, N. (2011): Numerical modeling of natural convection in an open cavity with two vertical thin heat sources subjected to a nanofluid. *International Communications in Heat and Mass Transfer*, vol. 38, pp. 110–118.

Maxwell, J. C. A. (1881): *Treatise Electricity Magn*. Second Ed., Clarendon Press, Oxford, UK.

Patankar, S. V. (1980): *Numerical Heat Transfer and Fluid Flow*, Hemisphere, Washington, DC.

Ooi, E. H.; Popov, V. (2013): Numerical study of influence of nanoparticle shape on the natural convection in cu-water nanofluid. *International Journal of Thermal Sciences*, vol. 65, pp. 178–188.

Ogut, E. B. (2009): Natural convection of water-based nanofluids in an inclined enclosure with a heat source. *International Journal of Thermal Sciences*, vol. 48, pp. 2063–2073.

Oztop, H., Abu-Nada, E., Varol, Y.; Al-Salem, K. (2011): Computational analysis of non-isothermal temperature distribution on natural convection in nanofluid filled enclosures. *Superlattices and Microstructures*, vol. 49, pp. 453–467.

Saleh, H.; Roslan, R.; Hashim, I. (2002): Natural convection heat transfer in a nanofluid-filled trapezoidal enclosure. *International Journal of Heat and Mass Transfer*, vol. 45, pp. 855–863.

Tiwari, R. K.; Das, M. K. (2007): heat transfer augmentation in a two-sided lid-driven differentially heated square cavity utilizing nanofluids. *International Journal of Heat and Mass Transfer*, vol. 50, pp. 2002–2018.